Electronic Supplementary Information

Rationally controlled helical organization of a multiple-hydrogen-bonding oligothiophene: guest-induced transition of helical-to-twisted ribbons

Shiki Yagai,*[a] Marina Gushiken,[a] Takashi Karatsu,[a] Akihide Kitamura,[a] Yoshihiro Kikkawa[b]

[a] *Department of Applied Chemistry and Biotechnology, Graduate School of Engineering, Chiba University, 1-33 Yayoi-cho, Inage-ku, Chiba 263-8522, Japan. Fax: +81-(0)43-290-3039; Tel: +81-(0)43-290-3368; E-mail: yagai@faculty.chiba-u.jp*

[b] *Photonics Research Institute, National Institute of Advanced Industrial Science and Technology (AIST), 1-1-1 Higashi, Tsukuba, Ibaraki 305-8562, Japan*

1. General methods

All reactions were performed under an atmosphere of nitrogen unless stated otherwise. All commercially available reagents and solvents were of reagent grade and used without further purification. Silica gel plates were 250 μm thick, 60 F_{254} grade from Merck. Silica gel was grade 60N (Spherical, Neutral, 60–210 mesh) from Kanto chemicals, Japan. ^{1}H NMR spectra were recorded on JEOL LA400 and BRUKER-DPX 300 spectrometers and chemical shifts were reported in ppm (δ) with the signal of TMS as internal standard. APCI mass spectra were recorded by Exactive (Thermo Fisher Scientific). UV/vis and fluorescence spectra were recorded on a JASCO V660 spectrophotometer and a JASCO FP6600 spectrofluorometer, respectively. IR spectra were recorded on a JASCO FT/IR-410. Circular and linear dichroism spectra were recorded on a JASCO J840 spectropolarimeter. The solvents for the spectroscopic measurements and the gelation experiments were all spectral grade and used without further purification. Molecular modeling calculations were performed on MacroModel version 9.0. AFM images of the nanostructures were acquired under ambient conditions using a Multimode Nanoscope IIIa (Veeco Instruments, Santa Barbara, CA) in tapping mode. Silicon cantilevers (OMCL-AC240TS-C2) with a spring constant of 2 N/m and frequency of 70 kHz (nominal value, Olympus, Japan) were used. AFM samples were prepared by spin-casting of methylcyclohexane solutions onto highly-oriented pyrolytic graphite (HOPG). TEM images were acquired by using Hitachi H-7600 TEM operating at 80 kV accelerating voltage. The samples were prepared by spin-coating of MCH solutions of **1** and **1**·**BMx** ([**1**] = 1 × 10^{-4} M) onto carbon coated copper grids (400 mesh). TEM images were obtained after staining with uranyl acetate followed by drying the sample in vacuum for 24 hours. Powder X-ray diffraction analysis was carried out with a Rigaku Rint-2200 X-ray diffractometer with monochromated $Cu_{K\alpha}$ radiation and temperature-controlled heating stage.

2. Synthesis and analytical data

Oligothiophene **1** was synthesized according to Scheme S1. Oligothiophene **2**[1] and cyanurate **4**[2] were synthesized according to the reported methods.

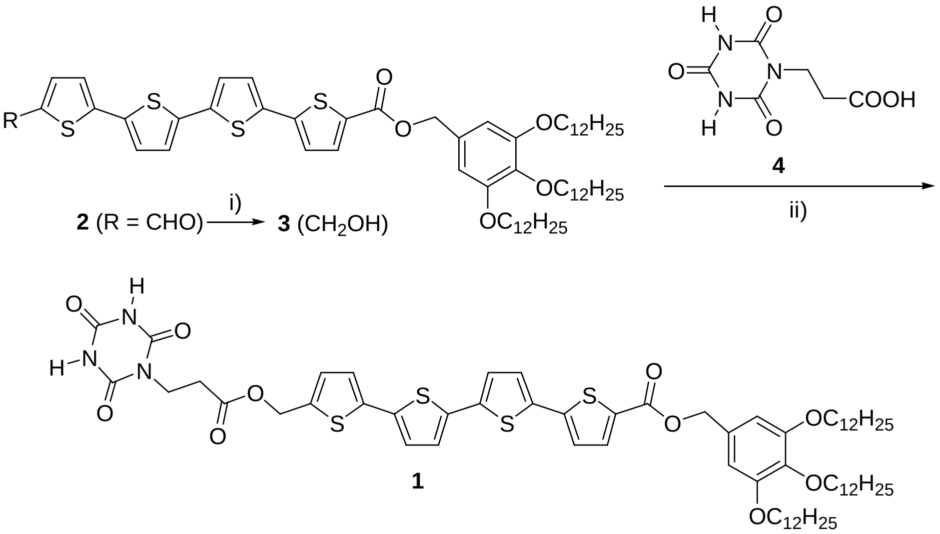

Scheme S1. Synthesis of cyanuric-acid-functionalized oligothiophene **1**. i) $NaBH_4$, THF, 85 %; ii) **4**, DMAP, WSC, THF, 20 %.

Oligothiophene **3**: To a THF solution (10 mL) of **2** (140 mg, 0.13 mmol), $NaBH_4$ (50 mg, 1.3 mmol) was added and the mixture was stirred for 1 h under N_2 atmosphere. The solvent was evaporated and the residue was dissolved in ethyl acetate and washed with water. Aqueous phase was further extracted with ether, and combined organic phases were washed with water for three times and dried with Na_2SO_4. After evaporation, the residue was purified by column chromatography over silica gel using chloroform as eluent to give **3** as yellow solid (120 mg, 85 %).

^{1}H NMR(300MHz $CDCl_3$) δ = 7.73–7.72 (d, J = 3.9 Hz, 1H), 7.19–6.93 (m, 7H), 5.23 (s, 2H), 4.83–4.81 (d, J = 6.0 Hz, 2H), 4.00–3.93 (m, 6H), 1.84–1.71 (m, 6H), 1.54–1.25 (m, 54H), 0.89–0.87 (m, 9H). HRMS (APCI): *m/z* calcd for $C_{61}H_{90}O_6S_4$ 1046.5615 [M^+], found 1046.5653.

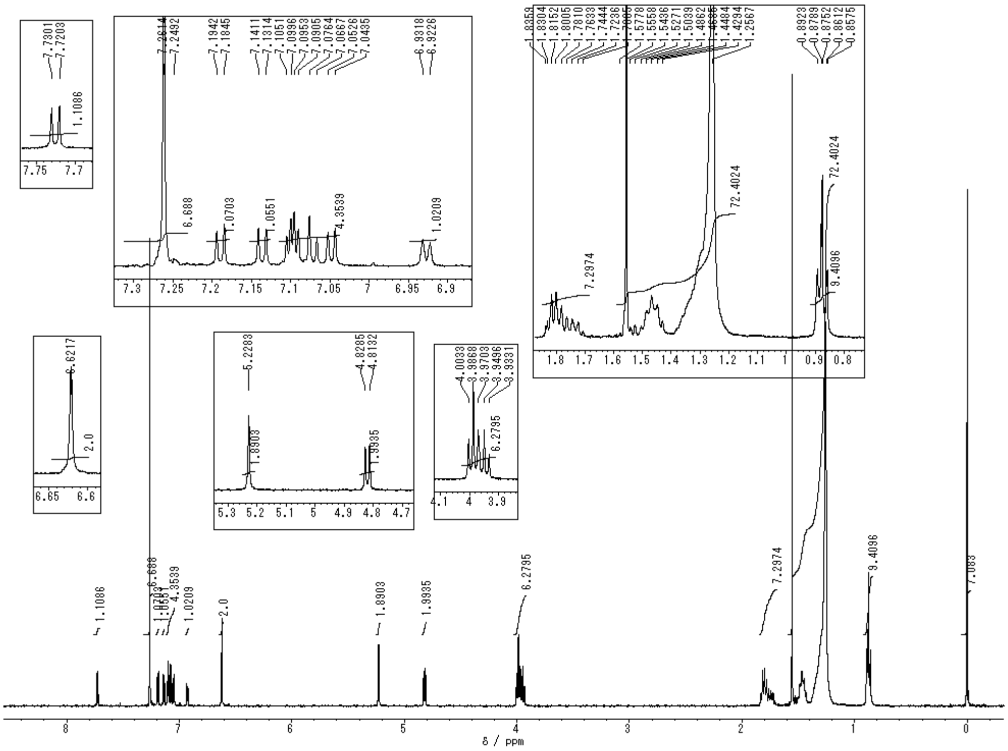

Chart 1. ^{1}H NMR spectrum of **3** in $CDCl_3$.

Oligothiophene **1**: Compound **3** was dissolved in dichloromethane, and stirred for 30 min under N_2 at 0 °C. 4,4-dimethylaminopyridine (18 mg, 0.152 mmol), and 1-ethyl-3-(3-dimethylaminopropyl)-carbodiimide hydrochloride (29 mg, 0.152 mmol) were added and the reaction mixture was warmed to r.t. and stirred overnight. The resulting mixture was washed twice with aq. HCl and twice with saturated aq. $NaHCO_3$. The organic layer was dried with Na_2SO_4, filtered and evaporated to dryness. The residue was purified by column chromatography over silica gel (eluent: $CHCl_3$/MeOH=100:0–99:1) and reprecipitated from a chloroform/methanol mixture. The resulting precipitates were collected by centrifugation to give pure compound **1** as yellow solid (0.022 g, 20%).

^{1}H NMR(400MHz, 5% DMSO/$CDCl_3$) δ= 10.81 (br., 2H), 7.73–7.72(d, J = 3.9 Hz, 2H), 7.20–7.00 (m, 7H), 6.62 (s, 2H), 5.22 (m, 2H), 4.16–4.12 (t, J = 7.3 Hz, 2H), 4.00–3.92 (m, 6H), 2.73–2.69 (t, *J* = 7.4 Hz, 2H), 1.81–1.72 (m, 6H), 1.49–1.26 (m, 54H), 0.89-0.86 (m, 9H). HRMS (APCI): *m/z* calcd for $C_{67}H_{95}O_{10}N_3S_4$ 1229.5895 [M^+], found 1229.5928.

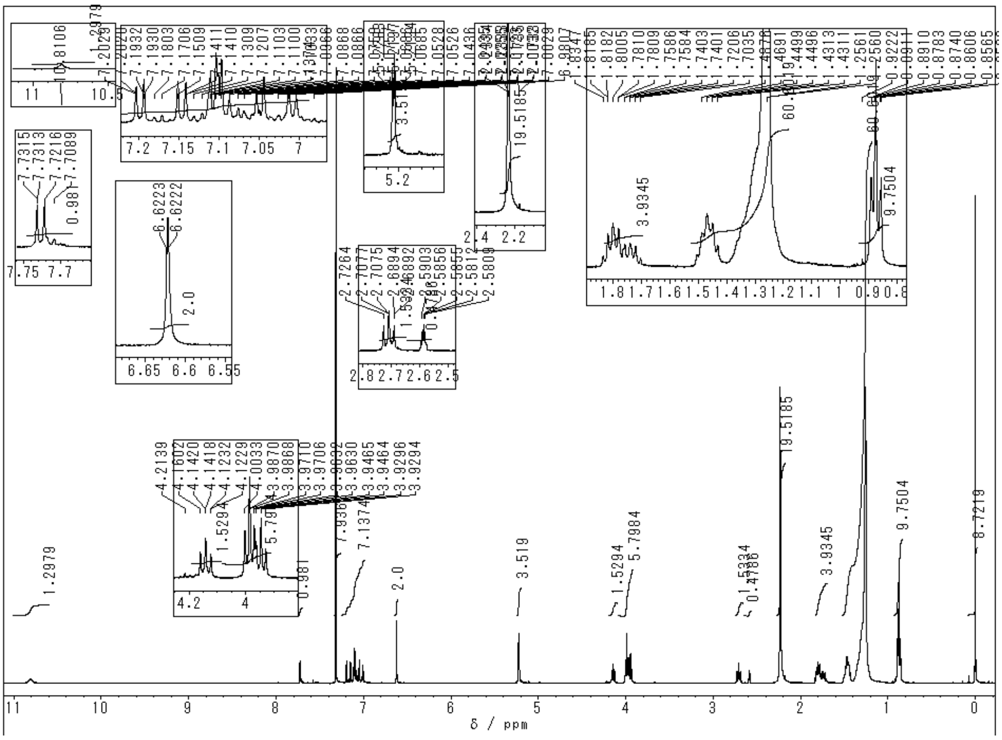

Chart 2. ^{1}H NMR spectrum of **1** in $CDCl_3$.

3. Supporting figures

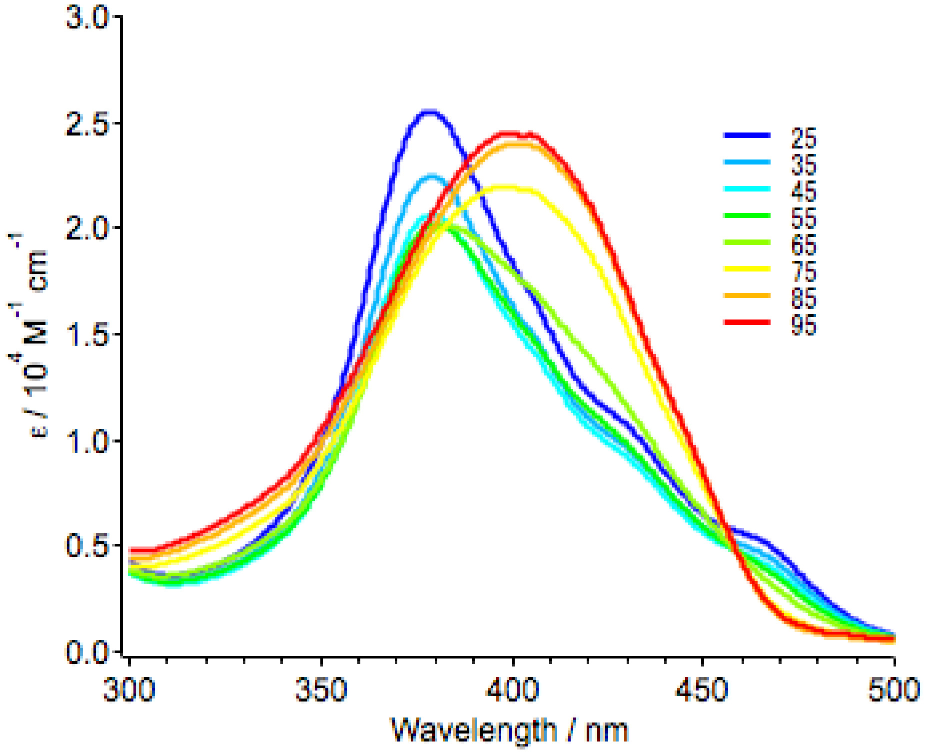

Fig. S1 Temperature-dependent (25–95 °C) UV/vis spectra of **1** in MCH ($c = 1.0 \times 10^{-5}$ M).

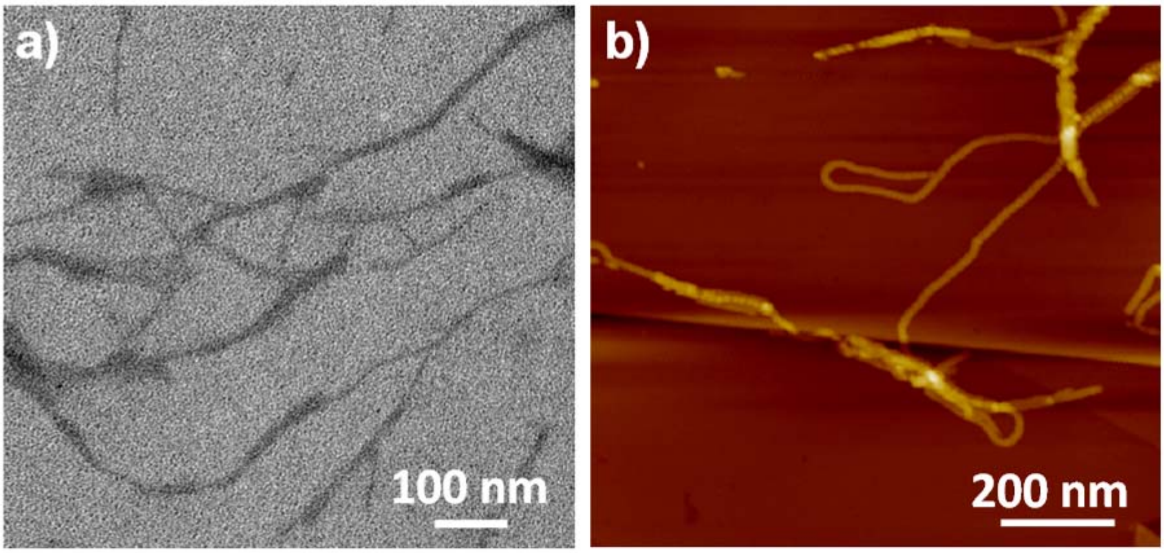

Fig. S2 a) TEM and b) AFM height images of nanostructures formed by **1** ($c = 1 \times 10^{-4}$ M) in MCH.

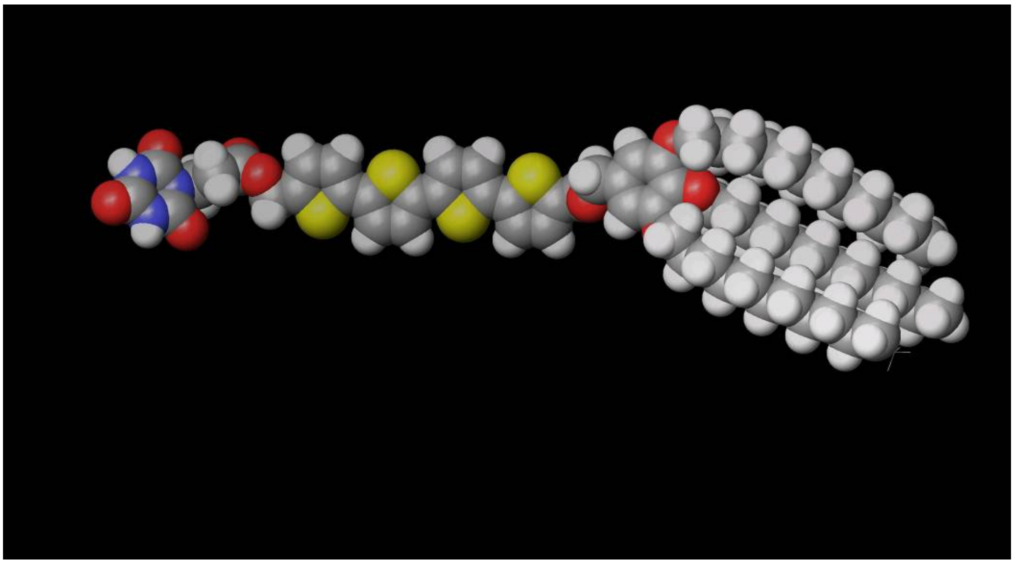

Fig. S3 CPK model of **1**. Energy-minimization was performed by MMFF calculation using Macromodel.

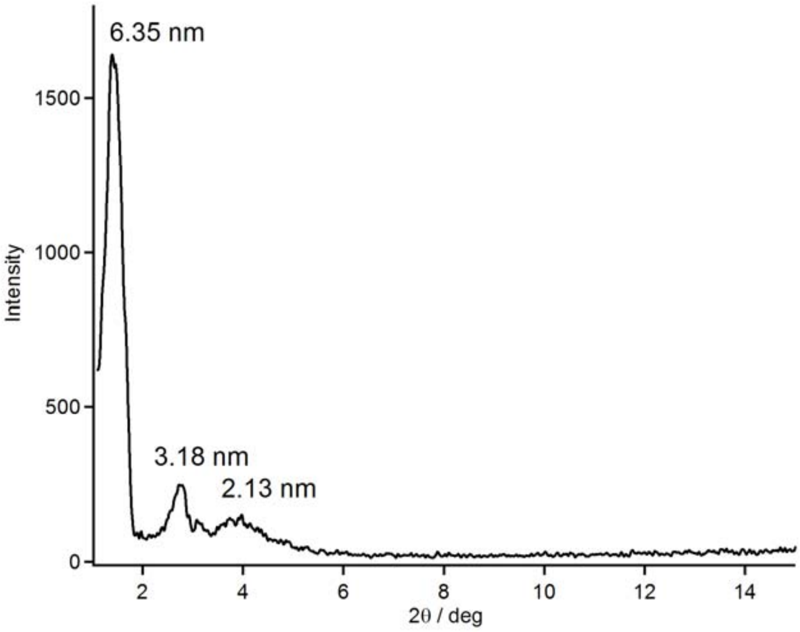

Fig. S4 X-ray diffraction pattern of **1** at 150 °C.

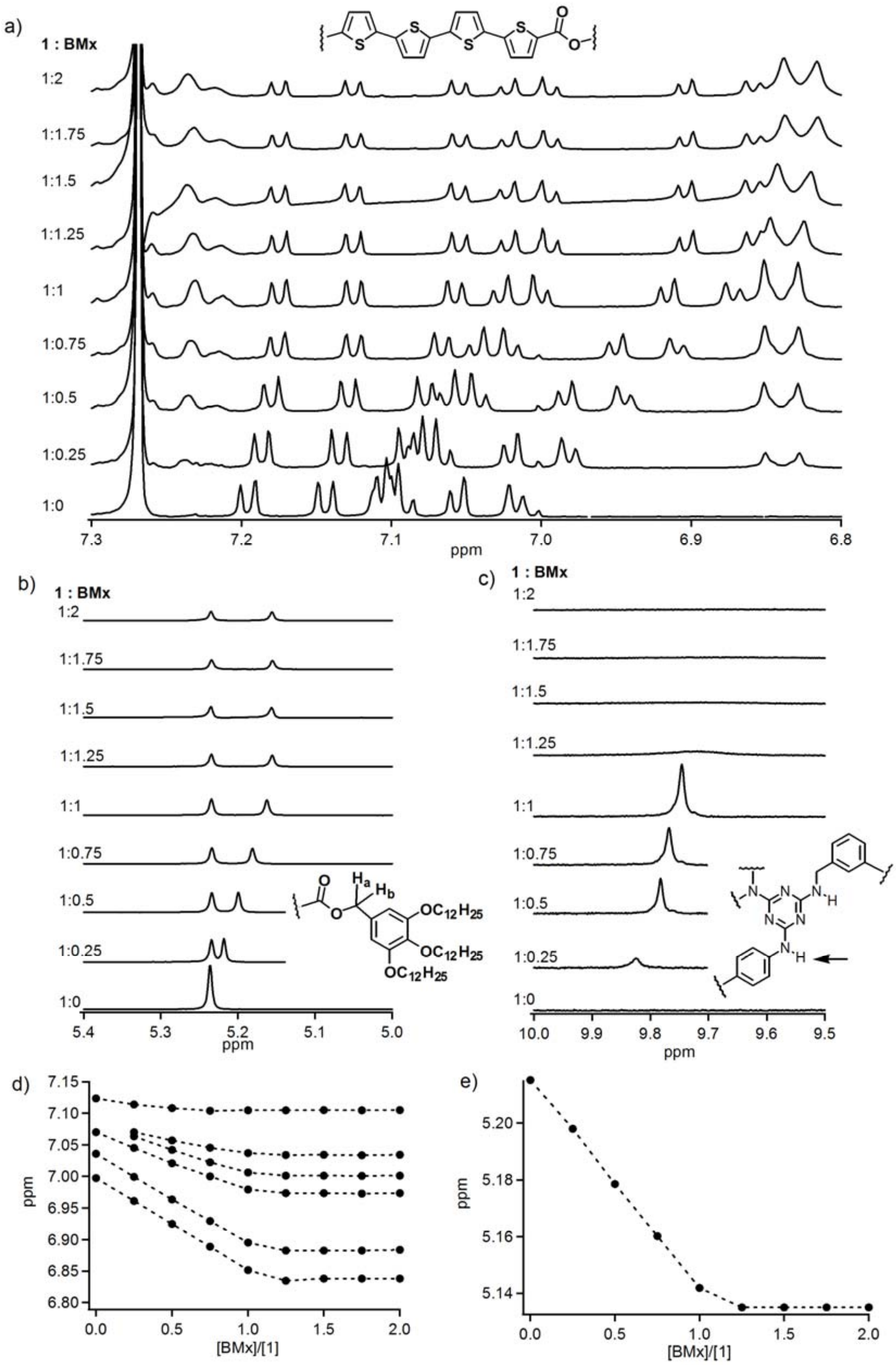

Fig. S5 a–c) Parts of ^{1}H NMR spectra of **1** ($c = 5 \times 10^{-3}$ M) in $CDCl_3$ in the presence of varying amounts of **BMx** (0 to 2 equiv.). d) Plot of chemical shifts of thiophene protons of **1** versus [**BMx**]/[**1**]. e) Plot of chemical shift of a benzyl proton of **1** versus [**BMx**]/[**1**].

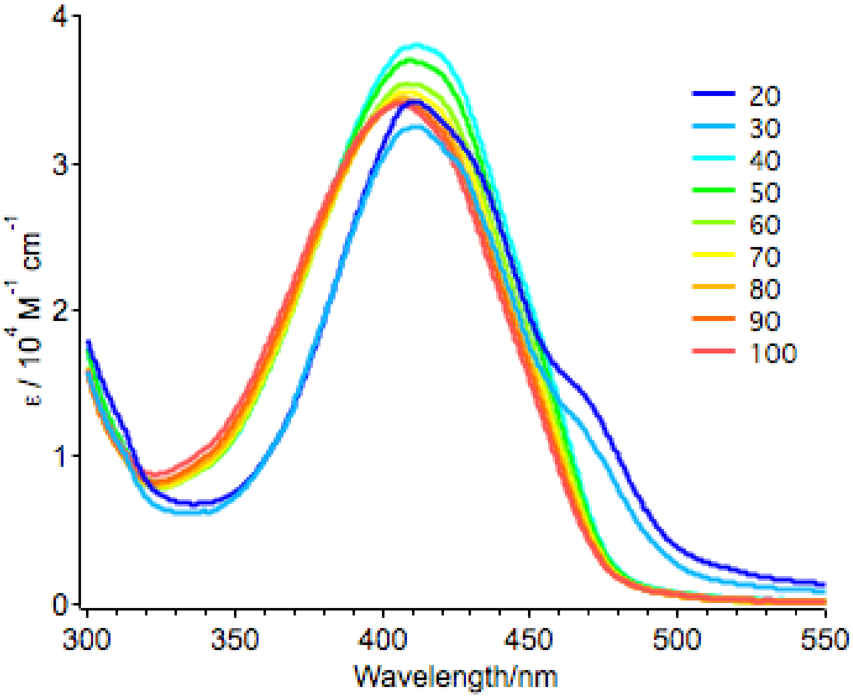

Fig. S6 Temperature-dependent (20–100 °C) UV/vis spectra of **1·BMx** in MCH ($c = 1.0 \times 10^{-5}$ M).

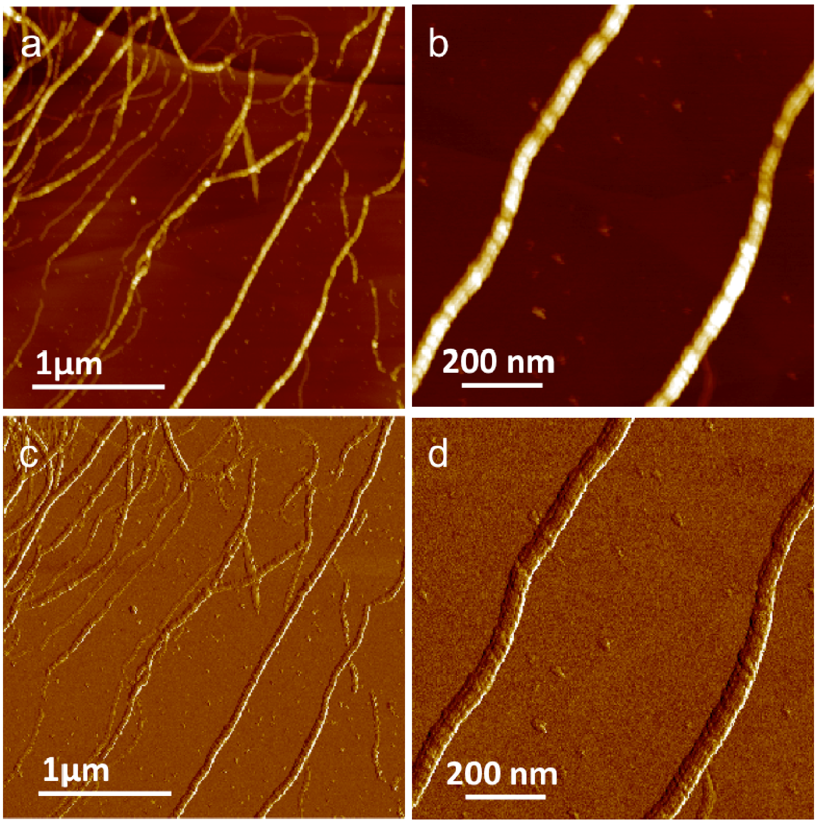

Fig. S7. a,b) AFM height and c,d) phase images of twisted ribbons of **1·BMx** ($c = 1 \times 10^{-4}$ M) spin-cast from MCH on HOPG.

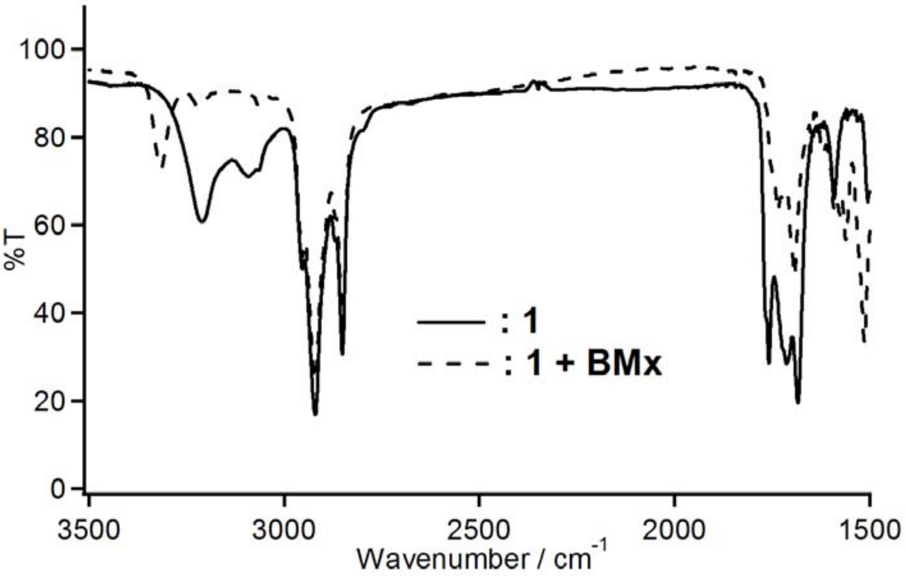

Fig. S8. FT-IR spectra of thin films of **1** and **1**·**BMx**.

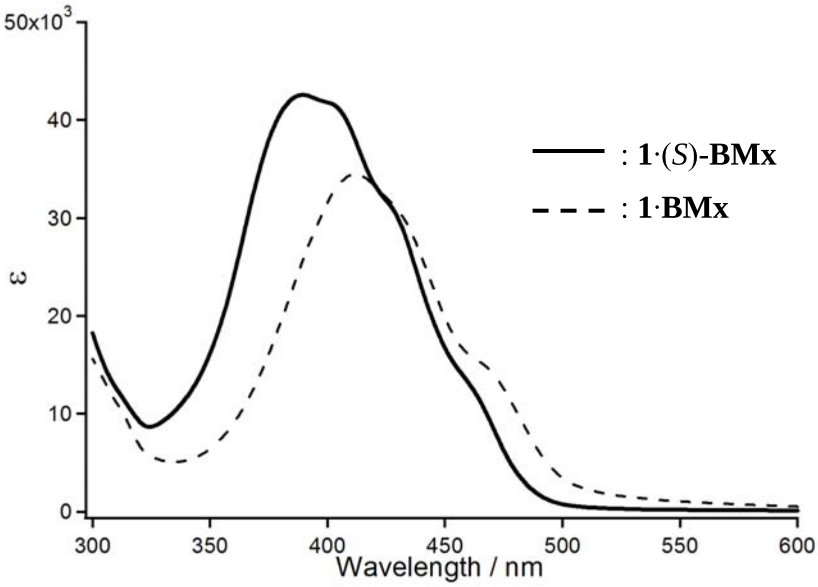

Fig. S9. Comparison of UV/vis spectra of chiral complex **1**·(*S*)-**BMx** ($c = 2 \times 10^{-5}$ M, solid curve) and achiral complex **1**·**BMx** ($c = 1 \times 10^{-5}$ M, dashed curve) in MCH.

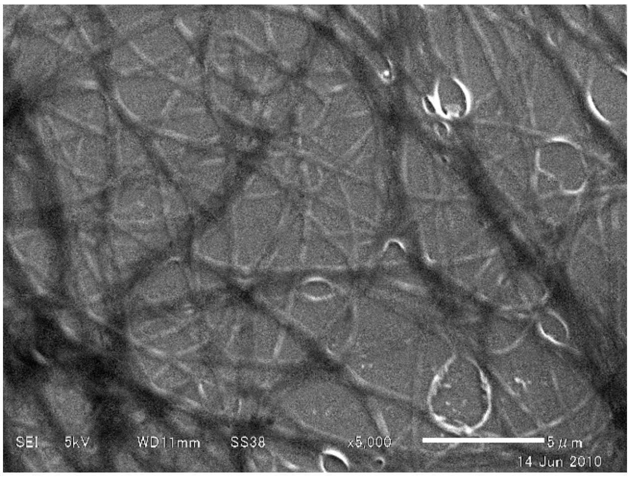

Figure S10. Scanning electron microscopic image of nanofibers of **1**·(*S*)-**BMx** formed in MCH solution ($c = 1 \times 10^{-4}$ M).

4. Reference

1) S. Yagai, T. Kinoshita, Y. Kikkawa, T. Karatsu, A. Kitamura, Y. Honsho and S. Seki, *Chem. Eur. J.*, 2009, **15**, 9320–9324.

2) a) M. Mascal, J. Hansen, P. S. Fallon, A. J. Blake, B. R. Heywood, M. H. Moore and J. P. Turkenburg, *Chem. Eur. J.*, 1999, **5**, 381–384. b) K. Hager, A. Franz and A. Hirsch, *Chem. Eur. J.*, 2006, **12**, 2663–2679.